# Splicing factor SRSF1 is indispensable for regulatory T cell homeostasis and function

**Takayuki Katsuyama**[1], **Vaishali R. Moulton**[1,2,*]

[1]Division of Rheumatology and Clinical Immunology, Department of Medicine, Beth Israel Deaconess Medical Center, Harvard Medical School, Boston, MA, USA

[2]Lead contact

## SUMMARY

The ability of regulatory T (Treg) cells to control the immune response and limit the development of autoimmune diseases is determined by distinct molecular processes, which are not fully understood. We show here that serine/arginine-rich splicing factor 1 (SRSF1), which is decreased in T cells from patients with systemic lupus erythematosus, is necessary for the homeostasis and proper function of Treg cells, because its conditional absence in these cells leads to profound autoimmunity and organ inflammation by elevating the glycolytic metabolism and mTORC1 activity and the production of proinflammatory cytokines. Our data reveal a molecular mechanism that controls Treg cell plasticity and offer insights into the pathogenesis of autoimmune disease.

## In brief

Katsuyama and Moulton show that splicing factor SRSF1 is indispensable for the homeostasis and function of Treg cells. Its conditional absence in Treg cells causes profound autoimmunity and organ inflammation by elevating glycolytic metabolism and production of proinflammatory cytokines. The study offers insights into the pathogenesis of autoimmune disease.

## Graphical Abstract

*Correspondence: vmoulton@bidmc.harvard.edu.

AUTHOR CONTRIBUTIONS

DECLARATION OF INTERESTS

The authors declare no competing interests.

SUPPLEMENTAL INFORMATION
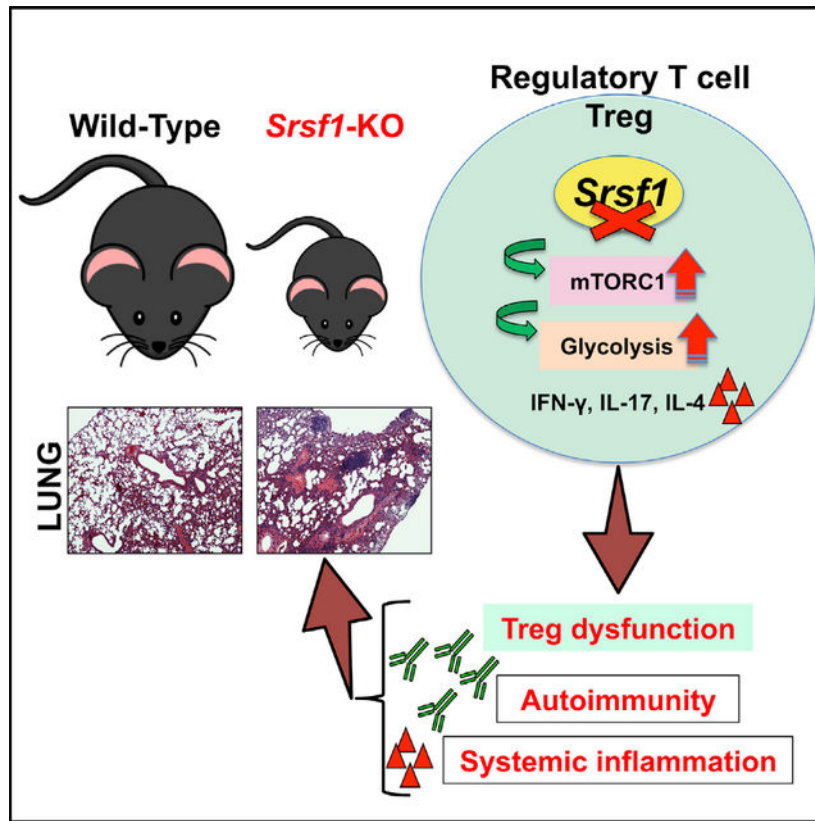
## INTRODUCTION

Regulatory T (Treg) cells are pivotal in maintaining self-tolerance to prevent fatal autoimmune disease (Plitas and Rudensky, 2016; Shevach, 2018; Wing et al., 2019). Defects in homeostasis, maintenance, and stability are key contributors to Treg cell dysfunction in mice and humans with autoimmune disease. Molecules and mechanisms that control Treg cell homeostasis and function are therefore critical determinants of Treg cell integrity and may serve as therapeutic targets for autoimmune disease (Kasper et al., 2016; Sharabi et al., 2018).

Instability and plasticity contribute to the defective function of CD4^{+}CD25^{+}Foxp3^{+} Treg cells and are known to play important roles in the pathogenesis of autoimmunity (Overacre and Vignali, 2016). Recent studies have shown that acquisition of effector-like properties and the production of proinflammatory cytokines from Treg cells is associated with not only their dysfunction but also pathogenic potential. It has been shown that Treg cells from patients with multiple sclerosis produce more interferon-$\gamma$ (IFN-$\gamma$) compared to those from healthy controls (Sumida et al., 2018), and IFN-$\gamma$-producing Treg cells exhibit suppressive dysfunction (Dominguez-Villar et al., 2011). Also, intereukin-17 (IL-17)-producing cells originating from Foxp3^{+} T cells have a key role in the pathogenesis of autoimmune arthritis (Komatsu et al., 2014). Furthermore, IL-17-producing Treg cells were found to be increased in the peripheral blood of patients with systemic lupus erythematosus (SLE) and associated with lupus nephritis and neuropsychiatric lupus (Jiang et al., 2019).

Metabolic programs have key roles in the function and stability of Treg cells. Treg cells rely on oxidative phosphorylation (OXPHOS) rather than glycolysis (Michalek et al., 2011; Newton et al., 2016). The mechanistic target of rapamycin (mTOR) pathway plays central roles in the glycolytic metabolism of Treg cells (Gerriets et al., 2016; Wei et al., 2016). Higher glycolytic metabolism induced by excessive mTOR complex 1 (C1) activity causes abnormal proinflammatory cytokine production from Treg cells and Treg dysfunction (Yu et al., 2018). However, the underlying mechanisms that control these pathways to regulate the stability and plasticity of Treg cells remain unclear.

Serine/arginine-rich splicing factor 1 (SRSF1) is the prototype member of the highly conserved serine/arginine (SR) family of RNA-binding proteins (Das and Krainer, 2014). SRSF1 controls post-transcriptional gene expression via pre-mRNA alternative splicing, mRNA stability, and translation (Howard and Sanford, 2015). While SRSF1 is a key controller of gene expression, very little is known of its role in the immune system and in immune-mediated disease. By discovery approaches, we identified SRSF1 to bind to the mRNA of the CD3 zeta (ζ) gene and promote its normal expression in human T cells (Moulton and Tsokos, 2010; Moulton et al., 2008). We demonstrated that SRSF1 is decreased in T cells from patients with SLE with severe disease (Kono et al., 2018; Moulton et al., 2013), which exhibit an overactive T cell phenotype (Katsuyama et al., 2018; Moulton and Tsokos, 2015; Tsokos, 2011). In agreement with these reports of its role in human autoimmune disease, we showed that selective deletion of SRSF1 in total T cells in mice leads to T cell hyperactivity and systemic autoimmunity in vivo (Katsuyama et al., 2019). While SRSF1 is an emerging molecule in the control of gene regulation and immune-mediated disease, its role in regulatory T cells is unknown.

Here, we show that mice that lack *Srsf1* in Treg cells develop early lethal systemic autoimmunity with peripheral organ inflammation. In the absence of SRSF1, Treg cells assume a proinflammatory phenotype and are unable to control lymphocyte activation. We find that *Srsf1*-deficient Treg cells display increased glycolytic metabolism and activity of the mTOR signaling pathway and produce proinflammatory cytokines. Our studies establish a crucial role of SRSF1 in the survival, integrity, and function of Treg cells and suggest that the deficiency of SRSF1 in Treg cells contributes to the pathogenesis of autoimmune disease. We propose that SRSF1 is requisite for the proper function of Treg cells and prevents their conversion to proinflammatory cells.

## RESULTS

### *Srsf1* deficiency in Treg cells leads to spontaneous early-onset fatal systemic autoimmune disease

To evaluate the role of SRSF1 in Treg cells, we crossed *Srsf1*-flox mice with the *Foxp3*$^{\text{YFP-cre}}$ mice to generate Treg conditional *Foxp3*$^{\text{YFP-Cre}}$*Srsf1*$^{+/+}$ wild-type (WT), *Foxp3*$^{\text{YFP-Cre}}$*Srsf1*$^{\text{flox/+}}$ heterozygous (HET), and *Foxp3*$^{\text{YFP-Cre}}$*Srsf1*$^{\text{flox/flox}}$ homozygous knockout (KO) mice. Treg *Srsf1*-KO mice succumbed to an early-onset fatal systemic autoimmune disease at 3–4 weeks of age (Figure 1A). Mice showed severely stunted in growth and significantly reduced body weight (Figures 1B and 1C). Mice exhibited signs of lymphoproliferative disease with splenomegaly and peripheral lymphadenopathy at 3

weeks of age (Figures 1D and 1E). Importantly Treg *Srsf1*-KO mice developed systemic autoimmunity. The titers of serum autoantibodies, including anti-double stranded DNA (anti-dsDNA) and anti-histone, were significantly higher in KO mice (Figure 1F). Notably, mice developed massive inflammatory cell infiltrations in the lungs with hemorrhages and destruction of alveolar structures (Figure 1G). Mice also exhibited inflammatory cell infiltration in the liver (Figure 1G). Flow cytometric analysis revealed significantly increased infiltrations of T cells and neutrophils in the lungs (Figure 1H). These results indicate that SRSF1 is essential for Treg cell physiology and that its loss leads to fatal systemic autoimmune inflammatory disease.

## Deletion of *Srsf1* in Treg cells leads to uncontrolled immune cell activation

Aberrant Treg homeostasis and/or function leads to unchecked immune cell activation (Georgiev et al., 2019). Given that the Treg *Srsf1*-KO mice succumb to autoimmune disease, we examined their peripheral lymphoid tissues for immune cell phenotype and function and found significantly expanded T cell populations in the spleen (Figure 2A), increased frequencies of $CD44^{hi}CD62L^{lo}$ effector/effector memory (EM) CD4 and CD8 T cell populations, and decreased proportions of $CD62L^{hi}CD44^{lo}$ naive CD4 and CD8 T cells in both spleen and peripheral lymph nodes (PLN) of Treg *Srsf1*-KO mice compared to WT mice (Figures 2B, 2C, S1A, and S1B). Deletion of *Srsf1* in Treg cells also led to increased production of proinflammatory cytokines. When stimulated *ex vivo*, CD4 T cells produced significantly higher IFN-$\gamma$ and IL-4 cytokines compared to WT mice (Figure 2D and E). Consistent with the observed systemic autoimmunity, $Fas^+GL7^+$ germinal center (GC) B cells were expanded in the spleens from KO mice (Figures 2F and 2G). To evaluate the effect of competitive WT Treg cells over the KO Treg cells, we performed mixed bone marrow chimera transfer experiments into $RAG^{-/-}$ mice. We observed that bone marrow chimera recipients exhibited milder phenotypic features with signs of peripheral T cell activation and autoimmunity without lethal systemic inflammation, suggesting that Treg cells from WT mice were able to rescue the severe phenotype observed in the Treg *Srsf1*-KO mice (Figures S2A and S2B). These data indicate that Treg-specific deletion of *Srsf1* leads to an uncontrolled peripheral immune cell activation and systemic autoimmune disease *in vivo*.

## SRSF1 is essential for not only survival but also function of Treg cells

SRSF1 is a pro-survival factor and controls genes involved in cell survival, and its deletion in cell lines *in vitro* leads to apoptosis (Bielli et al., 2014; Gautrey and Tyson-Capper, 2012; Li et al., 2005). We examined the Treg cell populations in Treg *Srsf1*-KO mice and found that the frequencies of Treg cells were dramatically reduced in the spleen, mesenteric lymph nodes (MLN), and peripheral lymph nodes (Figures 3A and 3B). In the thymus, the frequencies of $CD25^+Foxp3^+$ cells among single-positive CD4 cells were comparable between WT and Treg *Srsf1*-KO mice (Figure S3A), although the thymus was significantly reduced in size and cellularity in the KO mice. In addition, we observed increased frequencies of early apoptotic cells during induced Treg (iTreg) differentiation from naive CD4 T cells from Treg *Srsf1*-KO mice compared to those from WT mice (Figures 3C and 3D), with no significant difference in Foxp3 expression (Figure S3B). We also found that natural Treg (nTreg) cells from Treg *Srsf1*-KO mice exhibit increased

frequencies of dead cells compared to nTreg cells from WT mice (Figure S4A). To confirm that the survival defects of Treg cells in the Treg *Srsf1*-KO mice were not secondary to the massive inflammation observed in these mice, we analyzed the numbers of Treg cells in bone marrow chimera RAG$^{-/-}$ recipient mice that lacked the lethal systemic inflammation. Recoveries of CD45.2 Treg cells derived from the bone marrow cells of *Srsf1*-KO mice were significantly decreased compared to those from WT mice (Figure S4B). These results indicate that SRSF1 is intrinsically essential for Treg cell survival.

We then investigated the phenotypic characteristics of *Srsf1*-deficient Treg cells. Because of the diminished numbers of Treg cells in the Treg-*Srsf1*-KO mice, we utilized *Srsf1*-deficient Treg cells from T-cell-*Srsf1*-KO (*dLck*$^{Cre}$*Srsf1*$^{flox/flox}$) mice to obtain sufficient numbers. Treg suppressive function is associated with a number of molecules, including cytotoxic T lymphocyte antigen 4 (CTLA4), lymphocyte activation gene 3 protein (LAG3), glucocorticoid-induced tumor necrosis factor receptor-related protein (GITR), inducible costimulator (ICOS), Helios, CD39, and CD103 (Lu et al., 2017; Suffia et al., 2005; Vocanson et al., 2010). *Srsf1*-deficient Treg cells displayed lower frequencies of CTLA4$^+$ Treg cells and higher expression of PD-1 and CD39, whereas the expression levels of CD103, ICOS, GITR, Helios, and LAG3 were comparable to Treg cells from WT mice (Figures 4A and 4B). When we cultured fluorescence-activated cell sorting (FACS)-sorted nTreg cells with CD3 and CD28 antibodies for T cell receptor (TCR) engagement, Foxp3 expression was also comparable between WT and *Srsf1*-deleted Treg cells (Figures S5A and S5B).

To evaluate the role of SRSF1 in Treg function, we performed *in vitro* and *in vivo* Treg suppression experiments. To avoid the effects of systemic inflammation in the *FoxP3*$^{YFP-Cre}$*Srsf1*$^{flox/flox}$ Treg-*Srsf1*-KO mice, we performed these experiments using Treg cells from the *dLck*$^{Cre}$*Srsf1*$^{flox/flox}$ T cell *Srsf1*-KO mice. We confirmed that the frequencies of CD4$^+$CD25$^+$ cells and CD25$^+$FoxP3$^+$ Treg cells in T cell *Srsf1*-KO mice were comparable to those in WT mice (Figures S5C–S5F). CD4$^+$CD25$^+$CD127$^{lo}$ nTreg cells from T cell *Srsf1*-KO mice were unable to suppress the proliferation of conventional CD4 T (Tconv) cells in 7-day *in vitro* co-culture assays (Figures 4C and 4D). To investigate the function of *Srsf1*-deficient Treg cells *in vivo*, we adoptively transferred sorted WT or *Srsf1*-deficient Treg cells into B6 mice followed by a chemical-induced colitis with dextran sulfate sodium (DSS) administration. *Srsf1*-deficient Treg cells failed to suppress DSS-induced colitis, as assessed by loss of body weight and colon length shortening (Figures 4E and 4F). Furthermore, they failed to suppress colitis in the CD4-T-cell-transfer-induced colitis model in RAG$^{-/-}$ recipient mice (Figure 4G). These results indicate that SRSF1 plays an important role in Treg function and integrity.

To validate that SRSF1 plays an important role in Treg function distinct from its effect on survival, we evaluated the phenotype of the *Foxp3*$^{YFP-cre}$*Srsf1*$^{flox/+}$ Treg-*Srsf1*-HET mice. While these mice displayed normal frequencies of Treg cells in the spleen and mesenteric lymph nodes (Figures 5A and 5B), they exhibited signs of Treg dysfunction, as evidenced by the increased immune cell activation in the peripheral lymphoid tissues. Specifically, there were increased frequencies of activated CD69$^+$CD4 T cells in the peripheral lymphoid tissues compared to WT mice (Figures 5C and 5D). Furthermore, GC B cells were expanded

in the spleens of Treg *Srsf1*-HET mice compared to WT mice (Figures 5E and 5F). We also found that nTreg cells from Treg *Srsf1*-HET mice exhibit lower expression levels of CTLA4 similar to homozygous KO mice (Figure S6). These results indicate that SRSF1 plays an important role not only in the control of survival but also in the intrinsic function of Treg cells.

### *Srsf1* deficiency leads to an aberrant transcriptomics profile in Treg cells

To better understand the molecular landscape controlled by SRSF1, we performed RNA sequencing of *ex-vivo*-stimulated nTreg cells from WT and T cell *Srsf1*-KO mice followed by transcriptomics data analysis. We found that deletion of *Srsf1* led to significant transcriptional alterations in the *Srsf1*-deficient Treg cells. A total of 218 genes were differentially expressed (DE) in KO compared to WT Treg cells, with 65 genes upregulated and 153 genes downregulated at the 2-fold cutoff and 23 genes up and 8 genes down at the 4-fold cutoff ($p < 0.05$) (Figures 6A and 6B). Gene Ontology (GO) terms and Kyoto Encyclopedia of Genes and Genomes (KEGG) enrichment analysis revealed pathways involved in leukocyte differentiation, T cell activation, regulation of cell motility, and positive regulation of cytokine production (Figures 6C and 6D). Among these, the expression levels of multiple cytokines and chemokines, including IL-17A, IL-17F, CCL22, CCL20, CXCR3, and CCL17, were found to be elevated, and other genes, including SATB1, SCD1, and DAPL1, were decreased (Figure 6E). There was no significant difference in the expression levels of IL-10, IL-35, or transforming growth factor β (TGF-β). These data suggest that SRSF1 controls genes involved in activation, differentiation, migration, and cytokine production in Treg cells.

### *Srsf1* deficiency leads to Treg cell plasticity with a hyper-glycolytic metabolism and acquisition of an aberrant proinflammatory phenotype rescued by rapamycin

Recent studies have shown that the activated phenotype and production of proinflammatory cytokines from Treg cells is associated with their dysfunction in autoimmune diseases (Pandiyan and Zhu, 2015). Because the transcriptomics profiling indicated that SRSF1 controls genes involved in activation and cytokine production in Treg cells, we investigated cytokine production from the *Srsf1*-deficient Treg cells. We found that *Srsf1*-deficient Treg cells produced higher levels of proinflammatory cytokines, including IFN-γ, IL-17A, and IL-4, compared to WT Treg cells (Figures 7A and 7B). It is known that metabolic reprogramming influences the activation and function of Treg cells. Glycolytic metabolism promotes T helper cell type 1 (Th1) and Th17 differentiation (Peng et al., 2016; Shi et al., 2011). Moreover, higher glycolysis leads to abnormal proinflammatory cytokine production from Treg cells and Treg dysfunction (Sun et al., 2017). Therefore, we assessed the metabolic profiles of WT and *Srsf1*-deficient Treg cells. By glycolysis stress test assays, we found that *Srsf1*-deficient Treg cells had a significantly higher maximum glycolytic rate than WT Treg cells (Figures 7C and 7D). Activation of the mTORC1 pathway is known to induce higher glycolytic metabolism and abnormal proinflammatory cytokine production from Treg cells (Yu et al., 2018). Therefore, we evaluated the activity of the mTORC1 pathway. We found increased expression of phosphorylated S6 (pS6) protein levels, indicating an increased activity of the mTORC1 pathway (Figure 7E). Importantly, treatment with the mTOR inhibitor rapamycin reverted abnormal production of IFN-γ from *Srsf1*-deficient

Treg cells (Figures 7F and 7G). There was no difference in IL-17A production or Foxp3 expression after treatment with rapamycin in *Srsf1*-deleted iTreg cells (Figures S7A and S7B). Furthermore, we found that *Srsf1* mRNA expression levels as analyzed by RNA-sequencing data were comparable among naive CD4 T cells, effector CD4 T cells, and nTreg cells from WT mice (Figure S7C). These data suggest that SRSF1 regulates T cell plasticity, and in its absence, Treg cells convert to effector-like proinflammatory cells.

## DISCUSSION

In this study, we demonstrate that selective deletion of the essential RNA-binding protein SRSF1 in Treg cells leads to lethal systemic inflammation and autoimmunity. SRSF1 is not only necessary for Treg cell survival but also essential for a number of gene programs that are important in Treg function. Loss of SRSF1 in Treg cells results in impaired suppressive function and conversion to a proinflammatory phenotype. Glycolytic metabolism and mTOR pathway activity are increased in *Srsf1*-deficient Treg cells. Importantly, rapamycin treatment reverts the abnormal proinflammatory cytokine production. Thus, we show roles for SRSF1 in the control of Treg cell physiology and its potential role in the pathogenesis of autoimmune disease.

Recent advances in our understanding of molecules that regulate Treg survival and function have yielded insights into potential new therapeutic strategies for autoimmune diseases, including SLE (Mizui and Tsokos, 2018). There are conflicting reports on the numbers and function of Treg cells in autoimmune diseases and SLE, with some studies reporting defects in numbers and/or function and others reporting no differences (La Cava, 2018). Heterogeneity in patient cohorts, inclusion criteria, thresholds for disease activity, and differences in gating strategies for Treg cells account for these ambiguous results. A recent meta-analysis of a large number of studies, however, does point to reduced numbers of Treg cells in active patients with SLE (Li et al., 2019). Furthermore, recent clinical trials with low-dose IL-2 therapy boosted Treg numbers and improved disease activity in patients with SLE, indicating that targeting Treg cells is a valuable strategy to treat systemic autoimmune disease (He et al., 2016; von Spee-Mayer et al., 2016). Therefore, identifying molecules and mechanisms that promote Treg homeostasis and function is important. Our current study with Treg-specific conditional *Srsf1*-KO mice reveals that SRSF1 is crucial for not only Treg survival but also their integrity and function.

Recent studies have shown that increased activity of the mTOR pathway negatively affects Treg function (Chapman and Chi, 2015). Hyperactivation of the mTOR pathway induces higher glycolytic metabolic characteristics in Treg cells, which also leads to Treg dysfunction and production of proinflammatory cytokines (Apostolidis et al., 2016; Liu et al., 2010). Consistent with these reports, mTOR activation is implicated in rheumatic diseases (Perl, 2016, 2017), and rapamycin, an inhibitor of the mTOR pathway, promotes the expansion of functional Treg cells (Battaglia et al., 2006). Importantly, a recent clinical trial of rapamycin in patients with SLE has shown promising results (Lai et al., 2018). In this study, we demonstrate that the deletion of SRSF1 alters metabolic characteristics and leads to the activated phenotype of Treg cells via activation of the mTOR pathway. Therefore, while we have previously shown that decreased levels of SRSF1 are associated with worse

disease activity of patients with SLE (Moulton et al., 2013), here, we have uncovered a link between SRSF1 and Treg function.

Here, we found that *Srsf1*-deficient Treg cells exhibit significantly decreased expression of CTLA-4, which is crucial for the suppressive function of Treg cells (Wing et al., 2008). Because a constitutively active allele of the kinase Akt in Treg cells leads to an overall dampening of the Treg cell gene signature, including reduced expression of CTLA-4 (Haxhinasto et al., 2008), mTOR pathway activation might contribute to reduced expression levels of CTLA-4 in *Srsf1*-deficient Treg cells. However, PTEN-deficient Treg cells, which exhibited an activated mTOR pathway, showed higher expression levels of ICOS, PD-1, and GITR, whereas the expression of CTLA-4 was normal (Shrestha et al., 2015), suggesting the existence of other mechanisms by which SRSF1 controls CTLA-4 expression and reduces CTLA-4 expression may be another mechanism of impaired function of *Srsf1*-deficient Treg cells independent of the mTOR pathway. There might be other molecules controlled by SRSF1 that directly regulate the suppressive function of Treg cells independently of the phosphatidylinositol 3-kinase (PI3K)-AKT-mTOR pathway. Furthermore, how altered expression levels of immunosuppressive molecules including low CTLA-4 and high PD1 levels are associated with the impaired suppressive activity of *Srsf1*-deficient Treg cells in the context of inflammation needs further investigation.

Given the impaired homeostasis and survival of SRSF1-deficient Treg cells and ensuing autoimmunity, it would be important to carefully assess the survival/proliferation of these Treg cells in *in vitro* and *in vivo* functional studies and, furthermore, assess how these Treg cells respond to growth factor signals, including IL-2. Furthermore, it is important to identify the mechanisms underlying the impaired homeostasis and function to understand the role of SRSF1 in autoimmunity. Accordingly, we have recently shown that SRSF1 controls the expression of the anti-apoptotic gene Bcl-xL and that Bcl-xL levels are decreased in *Srsf1*-deficient T cells (Katsuyama et al., 2020). Furthermore, Bcl-xL is known to be important for development of functional regulatory CD4 T cells (Sharabi et al., 2010). We are currently pursuing mechanistic studies to evaluate the role of SRSF1/Bcl-xL-related pathways in Treg homeostasis and function. While the deficiency of SRSF1 leads to increased apoptosis, and this is certainly one aspect of its role in Treg homeostasis, it likely controls Treg function in addition through the control of genes involved in signaling and cytokine production, as we have recently shown (Katsuyama et al., 2019).

Also, further studies are required to assess the impact of SRSF1 on the thymic development of Treg cells. This will be better delineated using mice that lack SRSF1 in Treg cells but do not display severe inflammation or in mice with inducible deletion of SRSF1 so as to induce SRSF1 deletion in non-infant mice. Compared to homozygous Treg *Srsf1*-KO mice, *Srsf1*-HET mice display a significantly mild phenotype and normal frequencies of peripheral Treg cells, suggesting that thymic development in these mice may be normal. Yet, these *Srsf1*-HET mice exhibit signs of peripheral immune activation (Figures 5C–5F), suggesting that Treg cells are functionally defective. These data also suggest that there may be a gene-dose effect of the heterozygous versus homozygous deficiency of SRSF1 on Treg cell development and phenotype. This is pertinent from a translational standpoint, because while T cells from patients with SLE exhibit reduced levels of SRSF1, they do not completely

lack the gene. Therefore, *Srsf1*-HET mice maybe valuable tools to study Treg defects and translate findings to humans.

An interesting aspect of the systemic inflammation in the Treg *Srsf1*-KO mice is tissue involvement, with the lungs being a major site of severe inflammation. Given the differential expression of chemokine/receptor genes, it is likely that SRSF1 controls migratory capacity and tissue tropism of Treg cells, which determine tissue-specific inflammation. It would be important to evaluate the functional dynamics of *Srsf1*-deleted Treg cells to assess whether these Treg cells are dividing and producing inflammatory cytokines *in situ*. Since the metabolic cues are likely different across these different sites, they may induce different Treg cell functional outcomes. Also, while we observe a skewed proinflammatory cytokine phenotype of the Treg cells, we did not observe differences in the Treg signature cytokines. including IL-10 and TGF-β. While low CTLA4 expression may play a role in the *Srsf1*-mediated impairment of Treg function, the differential expression of chemokine/receptor genes suggests aberrant homing capacity and tissue localization of these Treg cells as potential mechanisms of defect. Additionally, from our results so far, it appears that SRSF1 does not control FoxP3 expression, because we do not see significant effect on FoxP3 levels after TCR engagement in nTreg cells or iTreg cells. Rather, SRSF1, through its control of apoptosis-related genes such as BcL-xL, CTLA4, mTOR signaling/inflammatory cytokine pathways, chemokine/receptor genes, and metabolism, likely controls Treg homeostasis, tissue-tropism, and suppressive function.

While we have evaluated cytokines in the experiments with rapamycin treatment, in further studies, we plan to assess other cytokines, including, among others, IL-4. We also plan to evaluate the mRNA levels of proinflammatory cytokines DE in the transcriptomics analyses. In the experiments to assess Treg function, we sorted cells based on the surface markers $CD4^+CD25^+CD127^-$ cells as nTreg cells. However, due to the severe systemic inflammation in the KO mice, these populations may contain activated T cells. Future evaluations using fluorescent-reporter-based sorting of cells, especially those from *Srsf1*-HET mice, would be valuable to overcome these issues.

Given the severe autoimmune phenotype in mice with Treg-specific deficiency of SRSF1, it is crucial to examine the expression levels of SRSF1 between Treg cells and conventional/effector T cells and the signals/factors that control its expression at the molecular level. We found that *Srsf1* mRNA levels are comparable between naive CD4, effector CD4, and nTreg cells (Figure S7C). The differences in phenotype we observed in our total T cell (Lck-Cre) *Srsf1*-KO (Katsuyama et al., 2019) versus Treg (FoxP3 Cre) *Srsf1*-KO mice is likely because of the timing of deletion. Under distal Lck-Cre promoter control, the *Srsf1* gene is deleted after thymic development, whereas in Treg-specific mice, it is deleted during early thymic development. Furthermore, while we have previously found its decreased levels in total T cells from patients with SLE (Katsuyama et al., 2019), studies are needed to evaluate SRSF1 levels in Treg cells from patients with SLE. While genome-wide association stuies (GWASs) in SLE have not specifically reported any SNPs in the *Srsf1* locus, we have considered environmental triggers, inflammatory milieu (cytokines), and hormones as potential factors in its regulation. We have initiated investigation on the underlying factors that control SRSF1 expression. We have shown that ubiquitin-induced proteasomal

degradation contributes to the downregulation of SRSF1 in T cells from normal individuals and patients with SLE (Moulton et al., 2014). We have ongoing studies investigating the role of estrogen in the regulation of SRSF1 at the transcriptional, post-transcriptional, and post-translational levels. In addition, post-transcriptional elements, including microRNAs, have been reported to modulate SRSF1 expression (Ramanujan et al., 2021; Sokół et al., 2018). In addition to its expression levels, the activity of SRSF1 and other SR proteins is controlled by phosphorylation, and these proteins are dephosphorylated by ceramide-induced protein phosphatase 1 (PP1). Ceramides are lipid metabolites generated by sphingomyelin hydrolysis, induced by various environmental triggers such as UV radiation, inflammatory cytokines (including tumor necrosis factor [TNF]), and cytotoxic drugs (Chalfant et al., 2002; Pettus et al., 2002). Thus, further studies are needed to delineate the precise role of these factors in regulating SRSF1 expression specifically in distinct T cell subsets.

In conclusion, we have uncovered a crucial role of SRSF1 in Treg homeostasis and function. Loss of SRSF1 leads to activation of the mTOR pathway, hyper-glycolytic metabolic phenotype, and proinflammatory cytokine production in Treg cells. Given the aberrant expression and function of SRSF1 in human systemic autoimmune disease, our findings suggest that low SRSF1 levels in Treg cells may play an important role in the pathogenesis of autoimmunity and implicate a therapeutic target for autoimmune diseases.

## STAR★METHODS

### RESOURCE AVAILABILITY

**Lead contact**—Further information and requests for reagents and resources should be directed to and will be fulfilled by the lead contact, Dr. Vaishali Moulton (vmoulton@bidmc.harvard.edu).

**Materials availability**—B6.$Srsf1^{fl/fl}$ (B6.$Srsf1$-flox) strain generated in this study will be deposited to Jackson Laboratory. B6.$Srsf1^{fl/fl}$d.Lck$^{cre}$ and B6.$Srsf1^{fl/fl}$Foxp3$^{YFP-cre}$ mice generated in this study will be made available on request with a complete Materials Transfer Agreement and we may require a payment if there is potential for commercial application.

**Data and code availability**—The RNA-sequencing data from this study have been deposited at the NCBI Gene Expression Omnibus (GEO) database under accession number GSE173268.

### EXPERIMENTAL MODEL AND SUBJECT DETAILS

**Mice**—C57BL/6J (stock 000664), B6.129S4-$Srsf1$-flox (stock 018020), B6.d.Lck$^{Cre}$ (stock 012837), B6.Foxp3$^{YFP-cre}$ (stock 016959) and RAG1$^{-/-}$ (stock 002216) mice were purchased from the Jackson Laboratory (Bar Harbor, Maine). B6.$Srsf1^{fl/fl}$ (B6.$Srsf1$-flox) mice were generated by backcrossing the B6.129S4-$Srsf1$-flox mice with C57BL/6J mice for twelve generations. They were then bred with B6.d.Lck$^{Cre}$ mice or B6.Foxp3$^{YFP-cre}$ mice to generate B6.$Srsf1^{fl/fl}$ d.Lck$^{Cre}$ (T cell $Srsf1$-KO) mice or B6.$Srsf1^{fl/fl}$ Foxp3$^{YFP-cre}$ (Treg $Srsf1$-KO) mice, respectively. Treg $Srsf1$-KO mice were used at 3–4 weeks old. In most

studies with Treg *Srsf1*-KO mice, sex-matched male and female WT littermates were used as controls. All mice were maintained in the specific pathogen free animal facility at Beth Israel Deaconess Medical Center (BIDMC). All studies were approved by the Institutional Animal Care and Use Committee at BIDMC.

## METHOD DETAILS

**Tissue processing and cell isolation**—Spleens and lymph nodes were homogenized using a syringe plunger and mesh cell strainer. RBC lysis was performed with ACK lysing buffer. All cell cultures were in RPMI complete medium (RPMI plus 10% FBS plus penicillin and streptomycin antibiotics). Blood samples from mice were collected by tail vein incision and capillary tube collection, and serum separated by centrifugation. For histopathology, tissues were immediately fixed in 10% formalin overnight, processed in an automated tissue processor, embedded into paraffin blocks and sent to the BIDMC Histopathology core for sectioning and slide staining with hematoxylin and eosin (H and E).

**Induced (i)Treg differentiation assays**—Naive CD4 T cells were isolated from spleens using the $CD4^+CD62L^+$ T cell isolation kit (Miltenyi Biotec) and cultured with anti-mouse CD3 (0.5 μg/ml) and anti-mouse CD28 (1 μg/ml) in the presence of recombinant (r)TGF-β (1ng/ml) and rIL-2 (20ng/ml) for 72 hours. For western blotting to detect phosphorylated (p)-S6, additional stimulation with anti-mouse CD3 (5 μg/ml) and anti-mouse CD28 (5 μg/ml) for 5min was performed.

**Flow cytometry**—Cells were washed with phosphate buffered saline (PBS) and stained with Zombie aqua viability dye. Surface staining was performed in FACS staining buffer (PBS plus 2% fetal bovine serum (FBS)) with Fc block on ice for 20 min. For intracellular cytokine staining, cells were stimulated for 4h in culture medium with PMA (100ng/ml), Ionomycin (1 μM) in presence of Monensin (1 μl/ml). Cells were surface stained followed by fixation and permeabilization. Appropriate antibodies were used for intracellular staining for cytokines or transcription factors. Flow cytometry data were acquired on CytoFLEX LX and analyzed with FlowJo software. All procedures were performed according to the manufacturer's instructions.

**Autoantibody detection**—For anti-double stranded (ds)DNA and anti-Histone ELISA, Immulon II plates (Dynatech) precoated with BSA were coated individually with 50 μg/ml calf thymus DNA (Sigma-Aldrich) or 50ug/ml calf thymus histone (Sigma-Aldrich) respectively. Serum was diluted and assayed for autoantigen reactivity against the plates described above by incubation overnight at 4°C. Bound IgG was detected with a goat polyclonal HRP–anti-mouse IgG detection antibody (SouthernBiotech) and visualized at 450nm using a tetramethylbenzidine (TMB) substrate (Sigma-Aldrich).

**Mixed bone marrow chimeras**—*Rag1*^{−/−} mice, 12–14 weeks of age were irradiated once at a total dose of 300rad for 4.25 s. Bone marrow cells from donor CD45.2 WT or Treg *Srsf1*-KO mice were mixed in a 1:1 ratio with BM cells from WT CD45.1 B6 mice and intravenously injected into the tail vein of irradiated *Rag1*^{−/−} recipient mice post irradiation

(a total of $8 \times 10^6$ cells/mouse). Recipient mice were euthanized 7–8 months after transfer and spleen cells analyzed by flow cytometry.

**RNA sequencing**—Total T cells were isolated from spleens of 8–10-week-old WT and T cell *Srsf1*-KO mice (n = 3 each). CD4+CD25+CD127lo natural (n) Treg cells were sorted by flow cytometry. nTregs were stimulated with anti-CD3 (2 μg/ml) and anti-CD28 (2 μg/ml) antibodies and rIL-2 (10 ng/ml) for 72h. Cells were collected, and total RNA was extracted using the RNeasy mini kit (QIAGEN) and submitted for RNA sequencing to the Molecular Biology Core Facilities at the Dana-Farber Cancer Institute (DFCI). Libraries were prepared using Illumina TruSeq Stranded mRNA sample preparation kits according to the manufacturer's protocols. Samples were sequenced on an Illumina NextSeq500 run with single-end 75-bp reads. Data analyses were performed using the VIPER pipeline by the DFCI Core.

**Western blot**—Total protein was extracted from cells after lysis with radioimmunoprecipitation assay (RIPA) buffer (Boston Bioproducts), electrophoresed on NuPAGE 4%–12% Bis-Tris gels (Life Technologies) and transferred to polyvinylidene fluoride (PVDF) membranes. Membranes were blocked with 5% (wt/vol) nonfat milk in Tris-buffered saline with 0.05% Tween 20 (TBS-T) for 1h, incubated with primary antibody (1:1000, or 1:10000 for β-actin antibody) in 5% milk in TBS-T or Hikari solution A (Nacalai Tesque) at 4°C overnight or at room temperature for 2h for β-actin antibody. Membranes were washed three times with TBS-T, incubated with HRP-conjugated secondary antibody (1:2000 for ECL detection reagents or 1:4000 for ECL prime detection reagents; GE Healthcare) for 1h, washed three times with TBS-T, developed with ECL reagents, and visualized by a Fujifilm LAS-4000 imager or a Bio-Rad ChemiDoc XRS imager. Densitometry was performed using Quantity One software (Bio-Rad).

***In vitro* suppression assays**—Total T cells were isolated from spleens by magnetic assisted cell sorting (MACS), using the Pan T cell isolation kit (Miltenyi Biotech). Cells were stained with fluorescent antibodies and CD4+CD25−CD127hi conventional CD4 T cells (Tconv) and CD4+CD25+CD127lo Tregs were sorted by flow cytometry (BD FACSAria II). Tconv cells ($6 \times 10^4$ cells/well) were labeled with CFSE and co-cultured with Treg cells at increasing ratios, in presence of Mitomycin C treated splenocytes ($12 \times 10^4$ cells/well) with anti-CD3 (5 μg/ml) and anti-CD28 (5 μg/ml) and crosslinker (goat anti hamster IgG, 10 μg/ml, MP Biomedicals) for seven days. Proliferation of Tconv cells was analyzed by flow cytometry.

***In vivo* Treg suppression assays**—Tconv cells and Tregs were sorted by flow cytometry as described above. For the dextran sulfate sodium (DSS) colitis induction, B6 mice at 14–18 weeks of age were administered 2.5% DSS (molecular weight 36–50 kDa; MP Biomedicals) in water for 7–10 days to induce colitis, and PBS or $7 \times 10^5$ Tregs from WT or T cell *Srsf1*-KO mice were injected intraperitoneally one day before the starting DSS. Body weight was measured every day for 8 days. Colon length was measured on the day of euthanasia. For the CD4 T cell transfer-induced colitis model, Rag1−/− mice were injected intravenously with $4 \times 10^5$ naive CD4 T cells along with either PBS or $2 \times 10^5$

Tregs from WT or T cell *Srsf1*-KO mice. Mice were weighed and examined once a week for 14 weeks.

**Metabolism assays**—Cell-Tak Cell and Tissue Adhesive (Fisher Scientific) was used for coating plates and $0.15 \times 10^6$ iTregs were seeded in each well. Extracellular acidification rate (ECAR) was measured using an 8-well XFp extracellular Flux Analyzer (Seahorse) following the Glycolytic stress test protocol.

## QUANTIFICATION AND STATISTICAL ANALYSIS

GraphPad Prism (version 6) was used for statistical analysis. Student's two-tailed t test, Mann-Whitney U test, and one-way analysis of variance (ANOVA) were used to calculate statistical significance among groups. All statistical details of experiments can be found in the figure legends. A *p* value of less than 0.05 was considered significant. Individual p values can be found in the figures.

## Supplementary Material

Refer to Web version on PubMed Central for supplementary material.

## ACKNOWLEDGMENTS

## REFERENCES

Apostolidis SA, Rodríguez-Rodríguez N, Suárez-Fueyo A, Dioufa N, Ozcan E, Crispín JC, Tsokos MG, and Tsokos GC (2016). Phosphatase PP2A is requisite for the function of regulatory T cells. Nat. Immunol. 17, 556–564. [PubMed: 26974206]

Battaglia M, Stabilini A, Migliavacca B, Horejs-Hoeck J, Kaupper T, and Roncarolo M-G (2006). Rapamycin promotes expansion of functional CD4+CD25+FOXP3+ regulatory T cells of both healthy subjects and type 1 diabetic patients. J. Immunol. 177, 8338–8347. [PubMed: 17142730]

Bielli P, Bordi M, Di Biasio V, and Sette C (2014). Regulation of BCL-X splicing reveals a role for the polypyrimidine tract binding protein (PTBP1/hnRNP I) in alternative 5′ splice site selection. Nucleic Acids Res. 42, 12070–12081. [PubMed: 25294838]

Chalfant CE, Rathman K, Pinkerman RL, Wood RE, Obeid LM, Ogretmen B, and Hannun YA (2002). De novo ceramide regulates the alternative splicing of caspase 9 and Bcl-x in A549 lung adenocarcinoma cells. Dependence on protein phosphatase-1. J. Biol. Chem. 277, 12587–12595. [PubMed: 11801602]

Chapman NM, and Chi H (2015). mTOR Links Environmental Signals to T Cell Fate Decisions. Front. Immunol. 5, 686. [PubMed: 25653651]

Das S, and Krainer AR (2014). Emerging functions of SRSF1, splicing factor and oncoprotein, in RNA metabolism and cancer. Mol. Cancer Res. 12, 1195–1204. [PubMed: 24807918]

Dominguez-Villar M, Baecher-Allan CM, and Hafler DA (2011). Identification of T helper type 1-like, Foxp3+ regulatory T cells in human autoimmune disease. Nat. Med. 17, 673–675. [PubMed: 21540856]

Gautrey HL, and Tyson-Capper AJ (2012). Regulation of Mcl-1 by SRSF1 and SRSF5 in cancer cells. PLoS ONE 7, e51497. [PubMed: 23284704]

Georgiev P, Charbonnier L-M, and Chatila TA (2019). Regulatory T Cells: the Many Faces of Foxp3. J. Clin. Immunol. 39, 623–640. [PubMed: 31478130]

Gerriets VA, Kishton RJ, Johnson MO, Cohen S, Siska PJ, Nichols AG, Warmoes MO, de Cubas AA, MacIver NJ, Locasale JW, et al. (2016). Foxp3 and Toll-like receptor signaling balance T$_{reg}$ cell anabolic metabolism for suppression. Nat. Immunol. 17, 1459–1466. [PubMed: 27695003]

Haxhinasto S, Mathis D, and Benoist C (2008). The AKT-mTOR axis regulates de novo differentiation of CD4+Foxp3+ cells. J. Exp. Med. 205, 565–574. [PubMed: 18283119]

He J, Zhang X, Wei Y, Sun X, Chen Y, Deng J, Jin Y, Gan Y, Hu X, Jia R, et al. (2016). Low-dose interleukin-2 treatment selectively modulates CD4(+) T cell subsets in patients with systemic lupus erythematosus. Nat. Med. 22, 991–993. [PubMed: 27500725]

Howard JM, and Sanford JR (2015). The RNAissance family: SR proteins as multifaceted regulators of gene expression. Wiley Interdiscip. Rev. RNA 6, 93–110. [PubMed: 25155147]

Jiang C, Wang H, Xue M, Lin L, Wang J, Cai G, and Shen Q (2019). Reprograming of peripheral Foxp3$^+$ regulatory T cell towards Th17-like cell in patients with active systemic lupus erythematosus. Clin. Immunol. 209, 108267. [PubMed: 31639448]

Kasper IR, Apostolidis SA, Sharabi A, and Tsokos GC (2016). Empowering Regulatory T Cells in Autoimmunity. Trends Mol. Med. 22, 784–797. [PubMed: 27461103]

Katsuyama T, Martin-Delgado IJ, Krishfield SM, Kyttaris VC, and Moulton VR (2020). Splicing factor SRSF1 controls T cell homeostasis and its decreased levels are linked to lymphopenia in systemic lupus erythematosus. Rheumatology (Oxford) 59, 2146–2155. [PubMed: 32206811]

Katsuyama T, Tsokos GC, and Moulton VR (2018). Aberrant T Cell Signaling and Subsets in Systemic Lupus Erythematosus. Front. Immunol. 9, 1088. [PubMed: 29868033]

Katsuyama T, Li H, Comte D, Tsokos GC, and Moulton VR (2019). Splicing factor SRSF1 controls T cell hyperactivity and systemic autoimmunity. J. Clin. Invest. 129, 5411–5423. [PubMed: 31487268]

Komatsu N, Okamoto K, Sawa S, Nakashima T, Oh-hora M, Kodama T, Tanaka S, Bluestone JA, and Takayanagi H (2014). Pathogenic conversion of Foxp3+ T cells into TH17 cells in autoimmune arthritis. Nat. Med. 20, 62–68. [PubMed: 24362934]

Kono M, Kurita T, Yasuda S, Kono M, Fujieda Y, Bohgaki T, Katsuyama T, Tsokos GC, Moulton VR, and Atsumi T (2018). Decreased expression of Serine/arginine-rich splicing factor 1 in T cells from patients with active systemic lupus erythematosus accounts for reduced expression of RasGRP1 and DNA methyltransferase 1. Arthritis Rheumatol. 70, 2046–2056. [PubMed: 29905030]

La Cava A (2018). Tregs in SLE: an Update. Curr. Rheumatol. Rep. 20, 6. [PubMed: 29464438]

Lai Z-W, Kelly R, Winans T, Marchena I, Shadakshari A, Yu J, Dawood M, Garcia R, Tily H, Francis L, et al. (2018). Sirolimus in patients with clinically active systemic lupus erythematosus resistant to, or intolerant of, conventional medications: a single-arm, open-label, phase 1/2 trial. Lancet 391, 1186–1196. [PubMed: 29551338]

Li X, Wang J, and Manley JL (2005). Loss of splicing factor ASF/SF2 induces G2 cell cycle arrest and apoptosis, but inhibits internucleosomal DNA fragmentation. Genes Dev. 19, 2705–2714. [PubMed: 16260492]

Li W, Deng C, Yang H, and Wang G (2019). The Regulatory T Cell in Active Systemic Lupus Erythematosus Patients: A Systemic Review and Meta-Analysis. Front. Immunol. 10, 159. [PubMed: 30833946]

Liu G, Yang K, Burns S, Shrestha S, and Chi H (2010). The S1P(1)-mTOR axis directs the reciprocal differentiation of T(H)1 and T(reg) cells. Nat. Immunol. 11, 1047–1056. [PubMed: 20852647]

Lu L, Barbi J, and Pan F (2017). The regulation of immune tolerance by FOXP3. Nat. Rev. Immunol. 17, 703–717. [PubMed: 28757603]

Michalek RD, Gerriets VA, Jacobs SR, Macintyre AN, MacIver NJ, Mason EF, Sullivan SA, Nichols AG, and Rathmell JC (2011). Cutting edge: distinct glycolytic and lipid oxidative metabolic programs are essential for effector and regulatory CD4+ T cell subsets. J. Immunol. 186, 3299–3303. [PubMed: 21317389]

Mizui M, and Tsokos GC (2018). Targeting Regulatory T Cells to Treat Patients With Systemic Lupus Erythematosus. Front. Immunol. 9, 786. [PubMed: 29755456]

Moulton VR, and Tsokos GC (2010). Alternative splicing factor/splicing factor 2 regulates the expression of the zeta subunit of the human T cell receptor-associated CD3 complex. J. Biol. Chem. 285, 12490–12496. [PubMed: 20118245]

Moulton VR, and Tsokos GC (2015). T cell signaling abnormalities contribute to aberrant immune cell function and autoimmunity. J. Clin. Invest. 125, 2220–2227. [PubMed: 25961450]

Moulton VR, Kyttaris VC, Juang Y-T, Chowdhury B, and Tsokos GC (2008). The RNA-stabilizing protein HuR regulates the expression of zeta chain of the human T cell receptor-associated CD3 complex. J. Biol. Chem. 283, 20037–20044. [PubMed: 18505733]

Moulton VR, Grammatikos AP, Fitzgerald LM, and Tsokos GC (2013). Splicing factor SF2/ASF rescues IL-2 production in T cells from systemic lupus erythematosus patients by activating IL-2 transcription. Proc. Natl. Acad. Sci. USA 110, 1845–1850. [PubMed: 23319613]

Moulton VR, Gillooly AR, and Tsokos GC (2014). Ubiquitination regulates expression of the serine/arginine-rich splicing factor 1 (SRSF1) in normal and systemic lupus erythematosus (SLE) T cells. J. Biol. Chem. 289, 4126–4134. [PubMed: 24368769]

Newton R, Priyadharshini B, and Turka LA (2016). Immunometabolism of regulatory T cells. Nat. Immunol. 17, 618–625. [PubMed: 27196520]

Overacre AE, and Vignali DA (2016). T(reg) stability: to be or not to be. Curr. Opin. Immunol. 39, 39–43. [PubMed: 26774863]

Pandiyan P, and Zhu J (2015). Origin and functions of pro-inflammatory cytokine producing Foxp3+ regulatory T cells. Cytokine 76, 13–24. [PubMed: 26165923]

Peng M, Yin N, Chhangawala S, Xu K, Leslie CS, and Li MO (2016). Aerobic glycolysis promotes T helper 1 cell differentiation through an epigenetic mechanism. Science 354, 481–484. [PubMed: 27708054]

Perl A (2016). Activation of mTOR (mechanistic target of rapamycin) in rheumatic diseases. Nat. Rev. Rheumatol. 12, 169–182. [PubMed: 26698023]

Perl A (2017). Review: Metabolic Control of Immune System Activation in Rheumatic Diseases. Arthritis Rheumatol. 69, 2259–2270. [PubMed: 28841779]

Pettus BJ, Chalfant CE, and Hannun YA (2002). Ceramide in apoptosis: an overview and current perspectives. Biochim. Biophys. Acta 1585, 114–125. [PubMed: 12531544]

Plitas G, and Rudensky AY (2016). Regulatory T Cells: Differentiation and Function. Cancer Immunol. Res. 4, 721–725. [PubMed: 27590281]

Ramanujan SA, Cravens EN, Krishfield SM, Kyttaris VC, and Moulton VR (2021). Estrogen-induced hsa-miR-10b-5p is elevated in T cells from patients with systemic lupus erythematosus and downregulates splicing factor SRSF1. Arthritis Rheumatol. Published online May 13, 2021. 10.1002/art.41787.

Sharabi A, Lapter S, and Mozes E (2010). Bcl-xL is required for the development of functional regulatory CD4 cells in lupus-afflicted mice following treatment with a tolerogenic peptide. J. Autoimmun. 34, 87–95. [PubMed: 19596183]

Sharabi A, Tsokos MG, Ding Y, Malek TR, Klatzmann D, and Tsokos GC (2018). Regulatory T cells in the treatment of disease. Nat. Rev. Drug Discov. 17, 823–844. [PubMed: 30310234]

Shevach EM (2018). Foxp3+ T Regulatory Cells: Still Many Unanswered Questions-A Perspective After 20 Years of Study. Front. Immunol. 9, 1048. [PubMed: 29868011]

Shi LZ, Wang R, Huang G, Vogel P, Neale G, Green DR, and Chi H (2011). HIF1alpha-dependent glycolytic pathway orchestrates a metabolic checkpoint for the differentiation of TH17 and Treg cells. J. Exp. Med. 208, 1367–1376. [PubMed: 21708926]

Shrestha S, Yang K, Guy C, Vogel P, Neale G, and Chi H (2015). Treg cells require the phosphatase PTEN to restrain TH1 and TFH cell responses. Nat. Immunol. 16, 178–187. [PubMed: 25559258]

Sokół E, K dzierska H, Czubaty A, Rybicka B, Rodzik K, Ta ski Z, Bogus1awska J, and Piekie1ko-Witkowska A (2018). microRNA-mediated regulation of splicing factors SRSF1, SRSF2 and hnRNP A1 in context of their alternatively spliced 3'UTRs. Exp. Cell Res. 363, 208–217. [PubMed: 29331391]

Suffia I, Reckling SK, Salay G, and Belkaid Y (2005). A role for CD103 in the retention of CD4+CD25+ Treg and control of Leishmania major infection. J. Immunol. 174, 5444–5455. [PubMed: 15845457]

Sumida T, Lincoln MR, Ukeje CM, Rodriguez DM, Akazawa H, Noda T, Naito AT, Komuro I, Dominguez-Villar M, and Hafler DA (2018). Activated β-catenin in Foxp3^{+} regulatory T cells links inflammatory environments to autoimmunity. Nat. Immunol. 19, 1391–1402. [PubMed: 30374130]

Sun L, Fu J, and Zhou Y (2017). Metabolism Controls the Balance of Th17/T-Regulatory Cells. Front. Immunol. 8, 1632. [PubMed: 29230216]

Tsokos GC (2011). Systemic lupus erythematosus. N. Engl. J. Med. 365, 2110–2121. [PubMed: 22129255]

Vocanson M, Rozieres A, Hennino A, Poyet G, Gaillard V, Renaudineau S, Achachi A, Benetiere J, Kaiserlian D, Dubois B, et al. (2010). Inducible costimulator (ICOS) is a marker for highly suppressive antigen-specific T cells sharing features of TH17/TH1 and regulatory T cells. J. Allergy Clin. Immunol. 126, 280–289.e1–7. [PubMed: 20624644]

von Spee-Mayer C, Siegert E, Abdirama D, Rose A, Klaus A, Alexander T, Enghard P, Sawitzki B, Hiepe F, Radbruch A, et al. (2016). Low-dose interleukin-2 selectively corrects regulatory T cell defects in patients with systemic lupus erythematosus. Ann. Rheum. Dis. 75, 1407–1415. [PubMed: 26324847]

Wei J, Long L, Yang K, Guy C, Shrestha S, Chen Z, Wu C, Vogel P, Neale G, Green DR, and Chi H (2016). Autophagy enforces functional integrity of regulatory T cells by coupling environmental cues and metabolic homeostasis. Nat. Immunol. 17, 277–285. [PubMed: 26808230]

Wing K, Onishi Y, Prieto-Martin P, Yamaguchi T, Miyara M, Fehervari Z, Nomura T, and Sakaguchi S (2008). CTLA-4 control over Foxp3+ regulatory T cell function. Science 322, 271–275. [PubMed: 18845758]

Wing JB, Tanaka A, and Sakaguchi S (2019). Human FOXP3^{+} Regulatory T Cell Heterogeneity and Function in Autoimmunity and Cancer. Immunity 50, 302–316. [PubMed: 30784578]

Yu X, Teng X-L, Wang F, Zheng Y, Qu G, Zhou Y, Hu Z, Wu Z, Chang Y, Chen L, et al. (2018). Metabolic control of regulatory T cell stability and function by TRAF3IP3 at the lysosome. J. Exp. Med. 215, 2463–2476. [PubMed: 30115741]

Author Manuscript

Author Manuscript

Author Manuscript

Author Manuscript

**Highlights**

- Deficiency of SRSF1 in Treg cells causes early lethal systemic autoimmune disease

- Treg cells from Srsf1-KO mice exhibit aberrant homeostasis and impaired function

- Srsf1-KO Treg cells display plasticity and produce aberrantly inflammatory cytokines

- Srsf1-KO Treg cells exhibit elevated glycolytic metabolism and mTOR activity
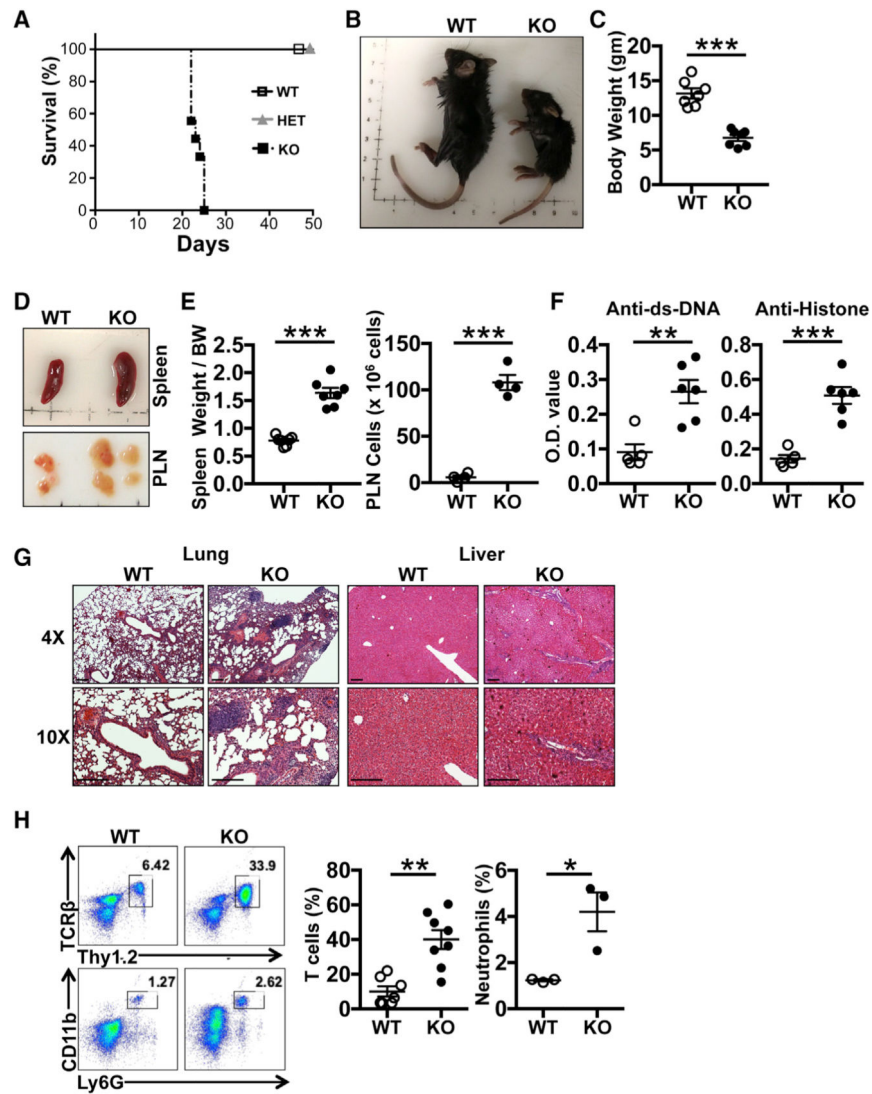
**Figure 1. Treg cell conditional *Srsf1*-KO mice spontaneously develop rapid fatal autoimmune disease**

(A) Percent survival of WT (*Foxp3*^YFP-Cre *Srsf1*^+/+), Treg *Srsf1*-HET (*Foxp3*^YFP-Cre *Srsf1*^flox/+), and Treg *Srsf1*-KO (*Foxp3*^YFP-Cre *Srsf1*^flox/flox) mice (n = 8–9 each).

(B) Representative images of 3-week-old WT and Treg *Srsf1*-KO mice.

(C) Graph shows body weight of WT and Treg *Srsf1*-KO mice (3–4 weeks old, age and sex matched, n = 7 each).

(D) Representative images of spleen and peripheral lymph nodes (PLNs) from 3-week-old WT and KO mice.

(E) Graphs show spleen weight/body weight (left, n = 7 each) and number of cells in PLNs (right, n = 4 each) (3–4 weeks old).

(F) Serum was collected from WT and Treg *Srsf1*-KO mice (3–4 weeks old). Autoantibodies were measured by ELISA (n = 5 WT, n = 6 KO).

(G) Representative images of hematoxylin and eosin staining of the lung and liver from 3- to 4-week-old WT and KO mice. Scale bars, 200 μM.

(H) Cells from lungs were analyzed by flow cytometry. Plots (left) and graphs (right) show infiltrating T cells and Ly6G$^+$CD11b$^+$ neutrophils in lungs from WT and Treg *Srsf1*-KO mice (T cells: n = 7 WT, n = 8 KO; neutrophils: n = 3 each; 3–4 weeks old).

*p < 0.05, **p < 0.005, and ***p < 0.0005, unpaired t test (C, E, F, and H); mean ± SEM.
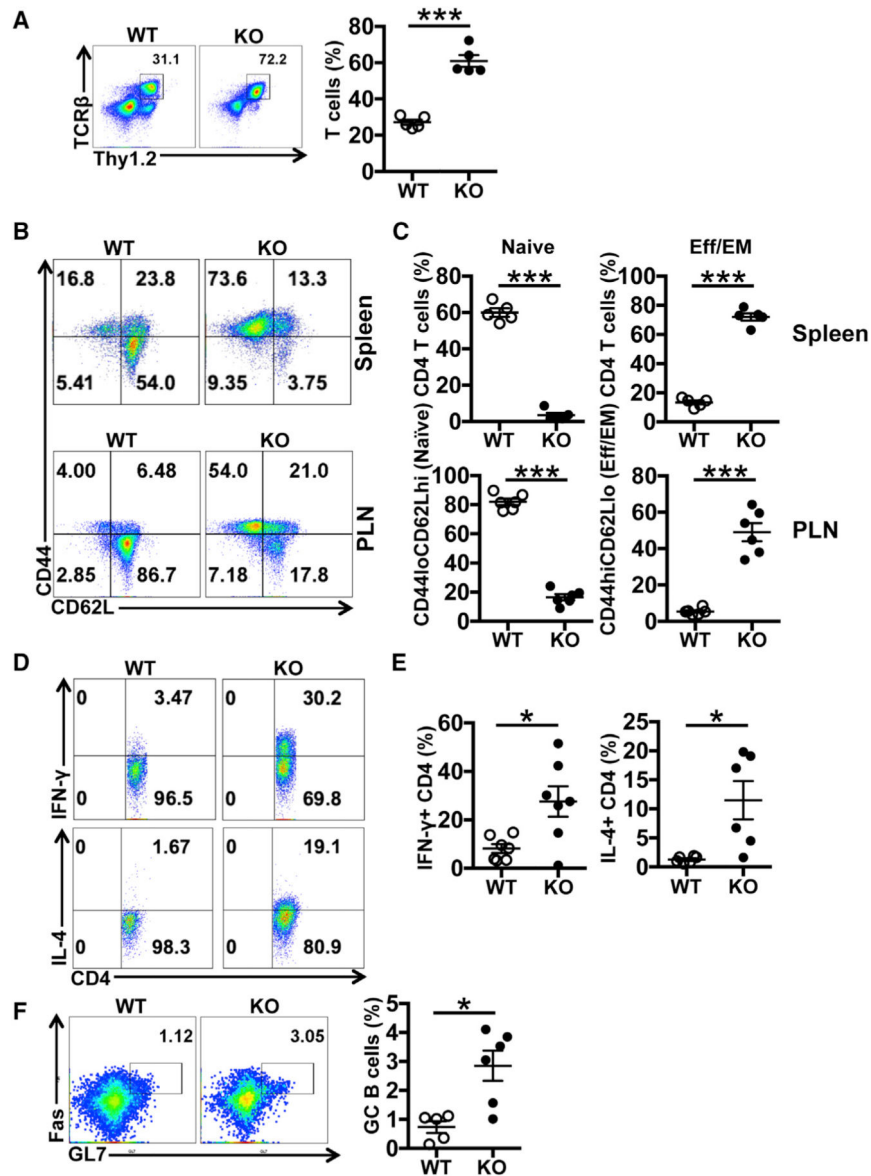
**Figure 2. Deletion of *Srsf1* in Treg cells results in peripheral immune cell activation**

Spleen cells were isolated from 3- to 4-week-old WT and Treg *Srsf1*-KO mice and analyzed by flow cytometry.

(A) Plots show Thy1.2$^+$TCRβ$^+$ T cells gated on live cells from spleen. Graph on the right shows the percentage of T cells (n = 5 each).

(B) Plots show CD62L and CD44 staining gated on live CD4 T cells in spleen and PLN from WT and KO mice.

(C) Graphs show the percentage of naive (CD44$^{lo}$ CD62L$^{hi}$) and effector/effector memory (CD44$^{hi}$ CD62L$^{lo}$) cells among CD4 T cells in spleen and PLN of WT and Treg *Srsf1*-KO (n = 5 each).

(D) Spleen cells were stimulated with phorbol myristic acid (PMA) and ionomycin with monensin for 4 h. Plots show IFN-γ- and IL-4-producing CD4 T cells.

(E) Graphs show the percentage of IFN-$\gamma$- and IL-4-producing CD4 T cells (IFN-$\gamma$: n = 7, IL-4: n = 6 each).

(F) Plots show GL7$^+$Fas$^+$ germinal center (GC) B cells gated on live B cells in spleen from WT and KO mice. Graph shows the percentage of GC B cells in spleen (n = 5 WT, n = 6 KO).

*p < 0.05 and ***p < 0.0005, unpaired t test (A, C, E, and F); mean ± SEM.
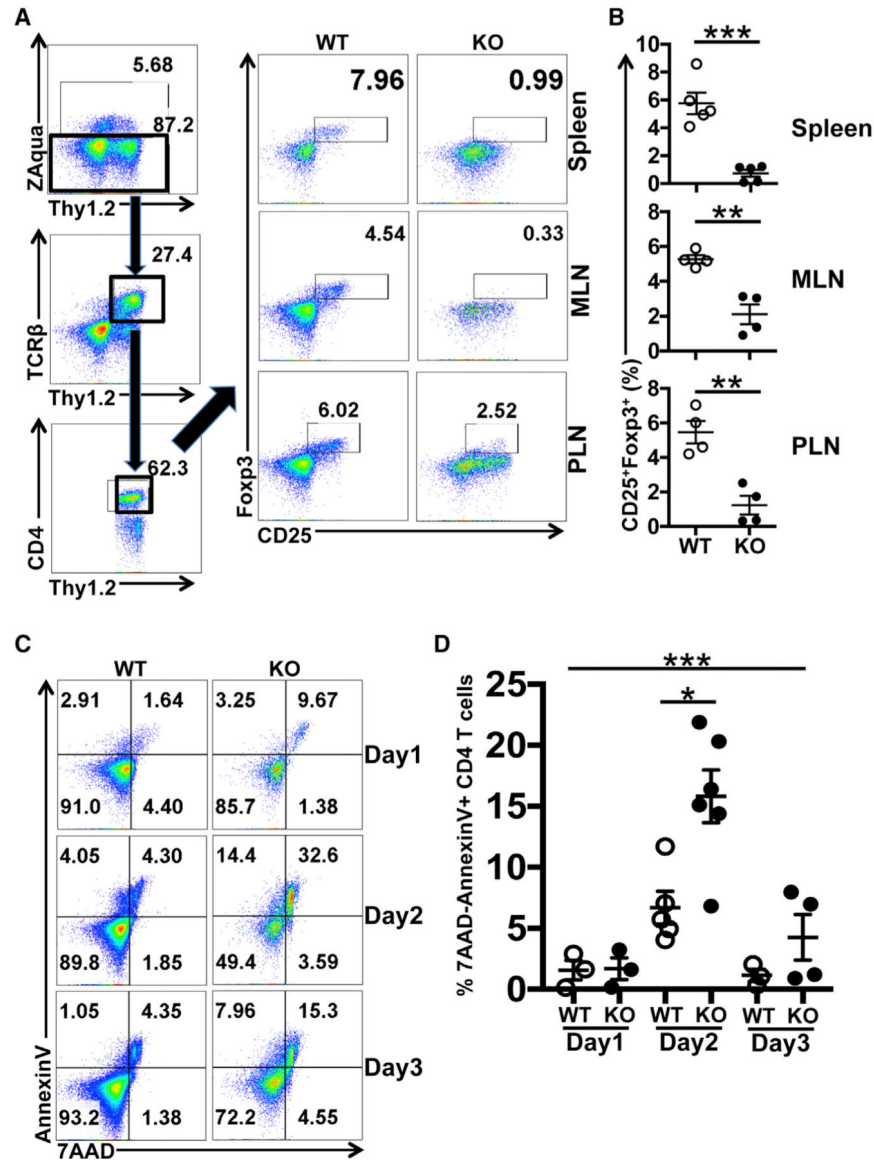
**Figure 3. SRSF1 is essential for survival of Treg cells**

(A) Plots show gating strategies and CD4⁺CD25⁺Foxp3⁺ Treg cells in spleen, MLN, and PLN from WT and Treg *Srsf1*-KO mice.

(B) Graphs show frequencies of CD4+CD25+Foxp3+ Treg cells (spleen: n = 5 each; MLN and PLN: n = 4 each).

(C) Naive CD4 T cells were isolated from pooled spleen and PLN cells from WT and Treg *Srsf1*-KO mice and cultured under Treg differentiation conditions. Cells were collected and analyzed by flow cytometry on days 1–3. Plots show 7AAD and Annexin V staining.

(D) Graph shows the percentage of early apoptotic (7AAD⁻Annexin V⁺) cells among CD4 T cells (n = 3–6).

*p < 0.05, **p < 0.005, and ***p < 0.0005, unpaired t test (B) or one-way ANOVA with Tukey's multiple comparisons test (D); mean ± SEM.
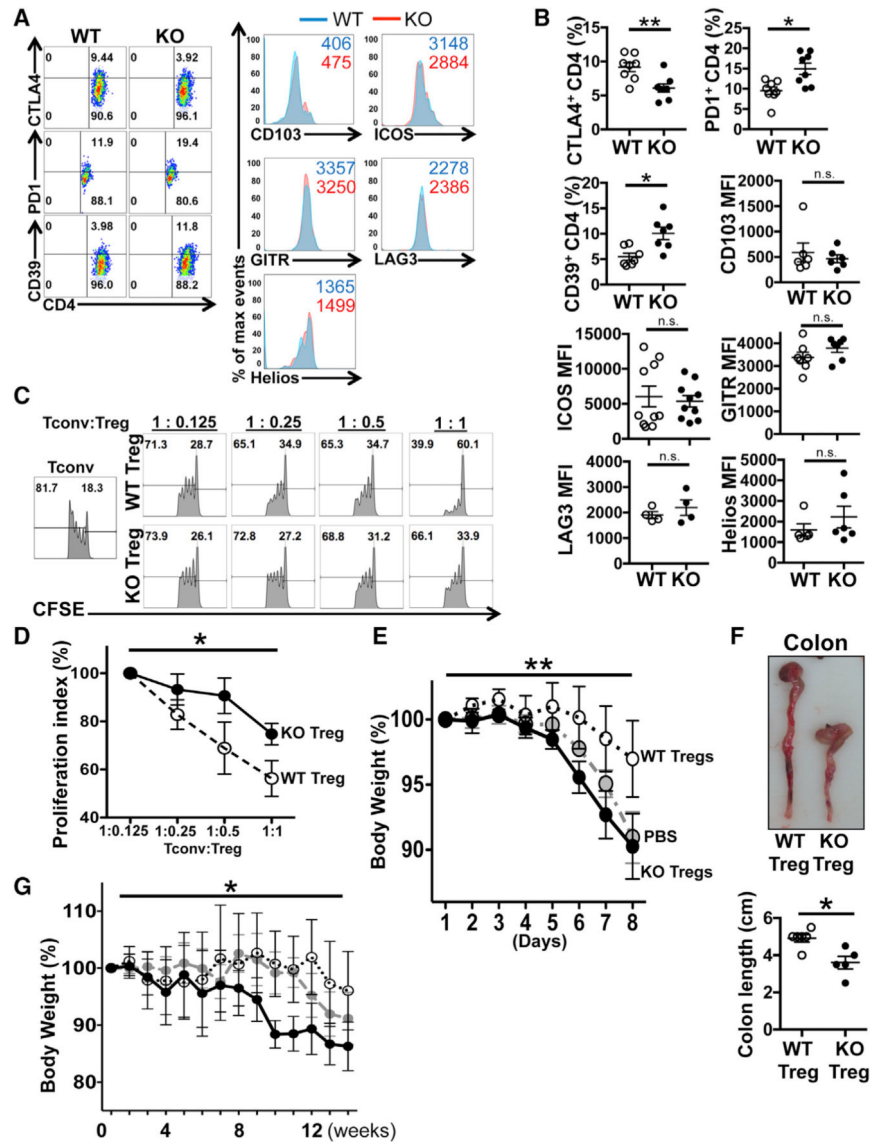
**Figure 4. *Srsf1*-deficient Treg cells exhibit impaired phenotype and suppressive function**

(A) Spleen cells were isolated from WT and T cell *Srsf1*-KO mice, and expression levels of Treg-associated molecules in CD4+CD25+Foxp3+ Treg cells were analyzed by flow cytometry. Dot plots (left) and histograms (right) show representative data of frequencies and mean fluorescence intensity (MFI) of markers in gated Treg cells.

(B) Graphs show the percentage of CTLA4+, PD1+, and CD39+ cells gated on Treg cells and quantification of MFI of CD103, ICOS, GITR, LAG3, and Helios (n = 4–10 each).

(C) Spleen cells from WT or T cell *Srsf1*-KO mice were isolated and conventional CD4 T (Tconv) cells and Treg cells (CD4+CD25+CD127lo) were sorted by flow cytometry. Tconv cells were labeled with carboxyfluorescein succinimidyl ester (CFSE) and co-cultured with Treg cells at increasing ratios for 7 days, and proliferation of Tconv cells was analyzed by flow cytometry. Representative plots are shown.

(D) Graph shows proliferation of Tconv cells (n = 8 WT, n = 10 KO).

(E) B6 mice were given 2.5% dextran sodium sulfate (DSS) in water to induce colitis for 8–10 days. One day before the initiation of DSS administration, PBS or flow-cytometry-sorted Treg cells (CD4$^+$CD25$^+$CD127$^{lo}$) from WT or T cell *Srsf1*-KO mice were injected into B6 mice. Graph shows body weight of mice from five independent experiments (n = 6 each).

(F) Representative image of colon after DSS administration for 8–10 days. Graph shows colon length of WT Treg and KO Treg group (n = 6 WT, n = 5 KO).

(G) Naive CD4 T cells were adoptive transferred into *Rag1*$^{-/-}$ mice to induce colitis together with PBS or sorted Treg cells (CD4$^+$CD25$^+$CD127lo) from WT or T cell *Srsf1*-KO mice. Graph shows time course of body weight of *Rag1*$^{-/-}$ recipient mice (n = 4–5 each).

*p < 0.05; **p < 0.005; and n.s., no significant difference, two-way ANOVA test (D, E, and G) and unpaired t test (B and F); mean ± SEM.
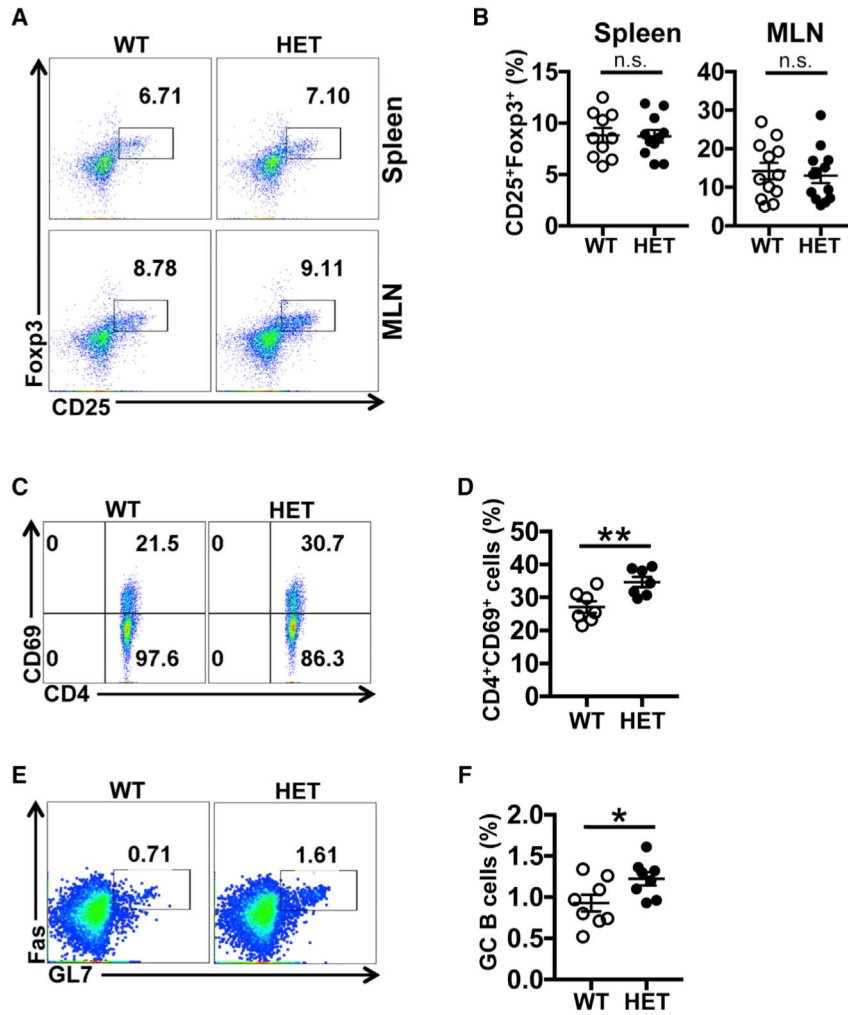
**Figure 5. Treg *Srsf1*-HET mice exhibit peripheral immune cell activation**

(A) Plots show CD4$^+$CD25$^+$Foxp3$^+$ Treg cells in spleen and MLN from WT and Treg *Srsf1*-HET (*Foxp3*$^{YFP\text{-}cre}$*Srsf1*$^{flox}$/+) mice.

(B) Graphs show frequencies of CD4$^+$CD25$^+$Foxp3$^+$ Treg cells among CD4 T cells in spleen and MLN (spleen: n = 10 WT and n = 11 HET; MLN: n = 12 WT and n = 13 HET).

(C) Plots show CD4$^+$CD69$^+$ cells in MLN from WT and Treg *Srsf1*-HET mice.

(D) Graph shows the percentage of CD4$^+$CD69$^+$ cells among CD4 T cells in MLN from 36- to 52-week-old WT and Treg *Srsf1*-HET mice (n = 7 each).

(E) Plots show GL7$^+$Fas$^+$ GC B cells gated on live B cells in spleen from WT and HET mice.

(F) Graph shows the percentage of GC B cells (n = 8 each).

*p < 0.05; **p < 0.005; and n.s., no significant difference, unpaired t test (B, D, and F); mean ± SEM.
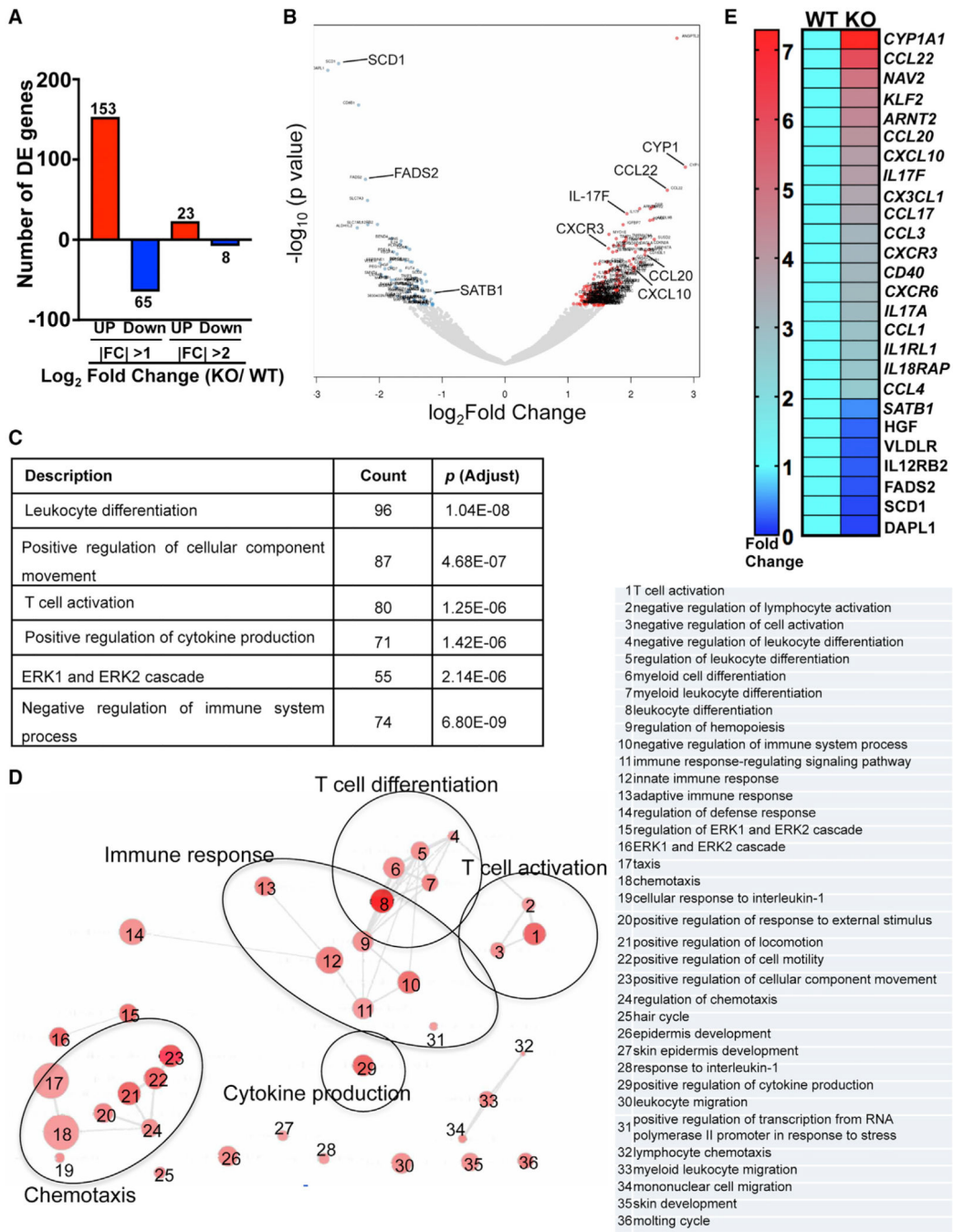
**Figure 6. *Srsf1*-deficient Treg cells display an aberrant transcriptomics profile**

Total T cells were isolated from spleens of 8- to 10-week-old WT and T cell *Srsf1*-KO mice (n = 3 each). Natural Treg (nTreg) cells (CD4$^+$CD25$^+$CD127$^{lo}$) were sorted by flow cytometry. nTreg cells were stimulated with anti-CD3, anti-CD28, and recombinant (r)IL-2 for 72 h.

(A) RNA-sequencing data analysis shows differentially expressed (DE) genes with log$_2$fold change (FC) differences at p < 0.05.

(B) Volcano plot showing upregulated and downregulated genes in KO nTreg cells.

(C) Table shows top pathways with gene counts identified by Gene Ontology (GO) term enrichment analysis of DE genes.

(D) GO terms enrichment map shows clusters of top 50 pathways. The size of red circles indicates the number of genes within a pathway, and color represents p values relative to the other displayed terms. Outlines (added manually) indicate groups of similar GO terms.

(E) Heatmap showing average expression of selected DE genes associated with T cell differentiation, cytokines, and chemokines.
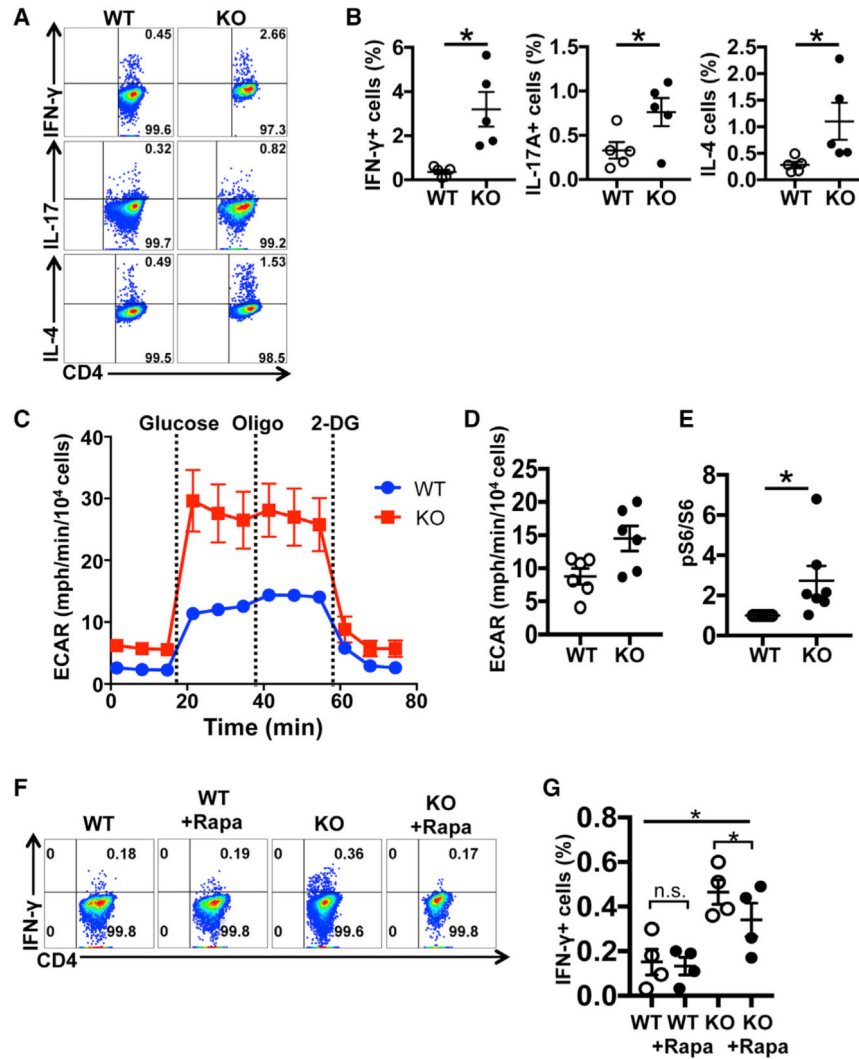
**Figure 7. *Srsf1* deficiency leads to Treg cell plasticity with hyper-glycolytic metabolism and acquisition of an aberrant proinflammatory phenotype rescued by rapamycin**

(A–H) Naive CD4 T cells were isolated from spleens of mice and cultured under Treg polarized condition for 72 h to generate induced Treg (iTreg) cells. (A) After 72 h, cells were stimulated with PMA and ionomycin with monensin, followed by surface and intracellular cytokine staining for flow cytometry. Plots show IL-17, IFN-γ, and IL-4 staining gated on CD4$^+$CD25$^+$Foxp3$^+$ Treg cells. (B) Graphs show the percentage of cytokine-producing cells among CD4$^+$CD25$^+$Foxp3$^+$ Treg cells (n = 5 each). (C) Glycolysis by induced Treg cells from WT and T cell *Srsf1*-KO mice was measured using extracellular acidification rate (ECAR) with injections glucose, oligomycin, and 2-Deoxyglucose (DG). Cells were counted for normalization. (D) Graph shows maximum glycolysis capacity calculated by subtracting the last measurement after 2-DG injection from the measurement before 2-DG injection (n = 6 each). (E) After 72-h polarization, additional stimulation with anti-CD3 (10 μg/mL) and anti-CD28 (10 μg/mL) for 5 min was performed. Total protein was immunoblotted for pS6 and total S6. Graph shows relative densitometry quantitation of pS6 and S6 (n = 7 each). (F) After 72-h polarization, iTreg cells were cultured for 4 h with PMA

plus ionomycin with or without rapamycin (10 nM). Cells were collected, surface stained, fixed, and permeabilized for intracellular cytokine staining. Plots show IFN-$\gamma$ intracellular staining gated on live Treg cells. (G) Graphs show average data from n = 4 mice in four independent experiments. *p < 0.05; and n.s., no significant difference, unpaired t test (B and E) or one-way ANOVA with Tukey's correction (G); mean ± SEM.

**KEY RESOURCES TABLE**

| REAGENT or RESOURCE | SOURCE | IDENTIFIER |
|---|---|---|
| Antibodies | | |
| Anti-mouse CD8a | Biolegend | Cat #100705 |
| | | RRID: AB_312744 |
| Anti-mouse CD25 | Biolegend | Cat #102012 |
| | | RRID: AB_312861 |
| Anti-mouse CD44 | Biolegend | Cat #103020 |
| | | RRID: AB_493683 |
| Anti-mouse CD62L | Biolegend | Cat #104412 |
| | | RRID: AB_313099 |
| Anti-mouse CD90.2 | Biolegend | Cat #140310 |
| | | RRID: AB_10643586 |
| Anti-mouse TCR-β | Biolegend | Cat #109205 |
| | | RRID: AB_313428 |
| Anti-mouse IL-4 | Biolegend | Cat #504109 |
| | | RRID: AB_493320 |
| Anti-mouse IL-17A | Biolegend | Cat #504109 |
| | | RRID: AB_493320 |
| Anti-mouse IFN-γ | Biolegend | Cat #505818 |
| | | RRID: AB_893526 |
| Biotin anti-mouse CXCR5 | Biolegend | Cat #145510 |
| | | RRID: AB_2562126 |
| Anti-mouse CD39 | Biolegend | Cat #143803 |
| | | RRID: AB_11219591 |
| Anti-mouse CD103 | Biolegend | Cat #121413 |
| | | RRID: AB_1227503 |
| Anti-mouse CD127 | Biolegend | Cat #135031 |
| | | RRID: AB_2564216 |
| Anti-mouse CTLA4 | Biolegend | Cat #106305 |
| | | RRID: AB_313254 |
| Anti-mouse GITR | Biolegend | Cat #120208 |
| | | RRID: AB_439726 |
| Anti-mouse ICOS | Biolegend | Cat #107705 |
| | | RRID: AB_313334 |
| Anti-mouse PD1 | Biolegend | Cat #135213 |
| | | RRID: AB_10689633 |
| Anti-mouse LAG3 | Biolegend | Cat #125207 |
| | | RRID: AB_2133344 |
| Anti-mouse Ly6G | Biolegend | Cat #127605 |

| REAGENT or RESOURCE | SOURCE | IDENTIFIER |
|---|---|---|
| | | RRID: AB_1236488 |
| Anti-mouse CD11b | Biolegend | Cat #101205 |
| | | RRID: AB_312788 |
| Anti-mouse GL7 | Biolegend | Cat #144614 |
| | | RRID: AB_2563292 |
| Annexin V | Biolegend | Cat #640941 |
| 7AAD | Biolegend | Cat #420404 |
| Anti-mouse CD4 | eBioscience | Cat #46-0041-82 |
| | | RRID: AB_11150050 |
| Anti-mouse Foxp3 | eBioscience | Cat #12-5773-82 |
| | | RRID: AB_465936 |
| Anti-mouse CD95 | BD Bioscience | Cat #12-5773-82 |
| | | RRID: AB_465936 |
| Purified anti-mouse CD3ε | Biolegend | Cat #100302 |
| | | RRID: AB_312667 |
| Purified anti-mouse CD28 | Biolegend | Cat #102112 |
| | | RRID: AB_312877 |
| Purified anti-mouse IFN-γ | Biolegend | Cat #505706 |
| | | RRID: AB_315394 |
| Purified anti-mouse IL-4 | Biolegend | Cat #504108 |
| | | RRID: AB_315322 |
| CD16/32 | Biolegend | Cat #101302 |
| | | RRID: AB_312801 |
| Anti-S6 ribosomal protein phospho-Ser 235 and Ser 236 | Cell Signaling Technology | Cat #2211S |
| Anti-S6 ribosomal protein | Cell Signaling Technology | Cat #2217S |
| Goat anti-rabbit IgG horseradish peroxidase (HRP) | Cell Signaling Technology | Cat #7074 |
| Goat anti-mouse IgG horseradish peroxidase (HRP) | Abcam | Cat #97023 |
| β-actin | Sigma-Aldrich | Cat #A5316 |
| Chemicals, peptides, and recombinant proteins | | |
| Rapamycin | Millipore | Cat #553210-100ug |
| Phorbol myristic acid (PMA) | Sigma-Aldrich | Cat #P1585 |
| Ionomycin | Sigma-Aldrich | Cat #I9657 |
| Mitomycin C | Sigma-Aldrich | Cat #m4287 |
| Dextran Sodium sulfate | MP Biomedicals | Cat #MP216011025 |
| Recombinant TGF-β | R&D systems | Cat #240-B-010 |
| Recombinant IL-2 | R&D systems | Cat #402-ML-100 |
| Critical commercial assays | | |
| Annexin binding buffer | Biolegend | Cat #422201 |
| Zombie Aqua Fixable Viability kit | Biolegend | Cat #423102 |

| REAGENT or RESOURCE | SOURCE | IDENTIFIER |
|---|---|---|
| Carboxyfluorescein succinimidyl ester Cell division Tracker Kit | Biolegend | Cat #423801 |
| Mouse regulatory T cell staining kit | eBioscience | Cat #88-8118-40 |
| Fixation/Permeabilization solution kit | BD Bioscience | Cat #554714 |
| Golgi Stop protein transport inhibitor | BD Bioscience | Cat #554724 |
| ACK lysing buffer | Fisher Scientific | Cat #1049201 |
| Mouse CD4$^+$CD62L$^+$ T cell isolation kit | Miltenyi Biotec | Cat #130-106-643 |
| Mouse Pan T cell isolation kit II | Miltenyi Biotec | Cat #130-095-130 |
| ECL detection reagent | GE Healthcare | Cat #RPN2209 |
| ECL prime detection reagent | GE Healthcare | Cat #RPN2236 |
| Deposited data | | |
| Raw and analyzed RNA-seq data | This paper | GEO: GSE173268 |
| Experimental models: organisms/strains | | |
| C57BL/6J mice | Jackson Laboratory | stock 000664 |
| B6.129S4-*Srsf1*-flox mice | Jackson Laboratory | stock 018020 |
| B6.d.Lck.Cre mice | Jackson Laboratory | stock 012837 |
| B6.Foxp3$^{YFP-cre}$ mice | Jackson Laboratory | stock 016959 |
| RAG1$^{-/-}$ mice | Jackson Laboratory | stock 002216 |
| B6.*Srsf1*$^{fl/fl}$ (B6-*Srsf1*-flox) mice | This paper | stock 036330 |
| B6.*Srsf1*$^{fl/fl}$ d.Lck$^{Cre}$ mice | This paper | N/A |
| B6.*Srsf1*$^{fl/fl}$ FoxP3$^{YFP-Cre}$ mice | This paper | N/A |
| Software and algorithms | | |
| FlowJo software | BD Biosciences | https://www.flowjo.com/ |
| GraphPad Prism version 6 | GraphPad | https://www.graphpad.com/ |
| Quantity One software | Bio-Rad | https://www.bio-rad.com/ |
| VIPER pipeline | DFCI Molecular Biology Core Facility | https://bitbucket.org/cfce/viper/src/master/ |